2021

Highly Dispersed Rh/NbOx Invoking High Catalytic Performances for the Valorization of Lignin Monophenols and Lignin Oil into Aromatics

Weixiang Guan

Xiao Chen

Chi Wing, Alex Tsang

Haoquan Hu

Changhai Liang

ACS Sustainable Chemistry & Engineering

pubs.acs.org/journal/ascecg

Research Article

Highly Dispersed Rh/NbO_x Invoking High Catalytic Performances for the Valorization of Lignin Monophenols and Lignin Oil into Aromatics

Weixiang Guan, Xiao Chen, Chi Wing Tsang, Haoquan Hu, and Changhai Liang*

Cite This: *ACS Sustainable Chem. Eng.* 2021, 9, 3529−3541

Read Online

ACCESS | Metrics & More | Article Recommendations | Supporting Information

ABSTRACT: As fossil fuels are constantly depleted, valorization of lignocellulosic biomass into valuable aromatic compounds is of great significance but exceedingly challenging. In this work, the structure and catalytic performance of various Rh/Nb_2O_5 catalysts were studied in detail via the catalytic hydrodeoxygenation of a representative lignin monophenol compound 2-methoxy-4-propylphenol. The best catalytic performance was obtained over Rh/Nb_2O_5-400 (Nb_2O_5 calcined at 400 °C) with an exceptional 98% yield of propylbenzene under 0.5 MPa H_2, which was mainly due to the cooperation between highly dispersed Rh metals and NbO_x species, in which Rh was responsible for dissociation of H_2 and NbO_x for breaking of C−O bonds at the metal−support interface. Besides, the lignin oil obtained in depolymerization of raw pine wood was directly used as the substrate in the catalytic hydrodeoxygenation reaction over the Rh/Nb_2O_5-400 catalyst under 0.5 MPa H_2. Encouragingly, the liquid products were identified and found that lignin oil was completely converted into C_6−C_{10} hydrocarbons (>99% selectivity) with an 80.1 mol % yield of aromatics. The results achieved in this work highlighted that high-value utilization of lignocellulosic biomass feedstocks to produce aromatic chemicals and liquid fuels could be achieved over Rh/Nb_2O_5 under a low hydrogen pressure.

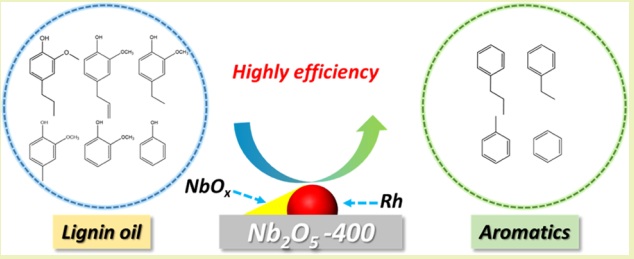

KEYWORDS: *2-methoxy-4-propylphenol, lignin oil, hydrodeoxygenation, Rh/Nb_2O_5, aromatics*

INTRODUCTION

Biomass is the only renewable organic carbon resource in nature when compared to other renewable resources, which provides a promising advantage to produce value-added products.[1] Lignocellulosic biomass is mainly composed of hemicellulose, cellulose, and lignin, accounting for 25−30 wt %, 35−50%, and 15−30 wt %, respectively.[2] Among these components, hemicellulose and cellulose are mainly composed of C5 and C6 sugars, while lignin is a three-dimensional amorphous polymer, which is composed of various types of phenylpropane units connected by C−C bonds and C−O bonds. Thereinto, hemicellulose and cellulose were widely used in production of biofuels and industrial fine chemicals.[3,4] However, lignin is commonly treated as waste in biorefinery processes due to its complex structure and high-refractory properties. In recent years, lignin has attracted researchers' interest because lignin is a potential resource for production of aromatic chemicals and liquid fuels, provided that suitable catalysts are sought.

Much work has been dedicated to depolymerization of lignin into valuable liquid products using various heterogeneous catalysts.[5−9] Among various liquid products, monophenols are regarded as the potential platform chemicals to produce high value-added products via hydrotreating processes.[7] However, these monophenols are not suitable for being directly used as fuels due to the high oxygen content and instabilities.[10] Therefore, extensive research studies have been focused on the hydrodeoxygenation of monophenols, such as phenol,[11,12] guaiacol,[13,14] *m*-cresol,[15] *p*-cresol,[16,17] etc.

It was widely accepted that 4-propylguaiacol was one of the main components of monophenols in the degradation of lignin.[2,18,19] For example, Tieuli et al. investigated hydrodeoxygenation of isoeugenol over Ni-SBA-15 with a 75% yield of propylcyclohexane at 300 °C and 3.0 MPa H_2.[10] Song et al. studied the demethoxylation of 4-propylguaiacol over MoO_3/SiO_2 and more than 80% selectivity of 4-propylphenol was achieved.[20] Yohe and co-workers developed a PtMo/MWCNT bimetallic catalyst and used it in the hydrodeoxygenation of dihydroeugenol with a 98% yield of propylcyclohexane.[21] It should be emphasized that hydrodeoxygenation of monophenols generally needs high hydrogen pressure, resulting in excessive hydrogen consumption, overhydrogenation, and

Received: November 19, 2020
Revised: February 5, 2021
Published: February 25, 2021

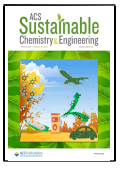

crack problems.[22] Therefore, catalytic upgrading of monophenols under low H_2 pressure emerged as a promising strategy to produce aromatic products in the point of view of avoiding aforementioned problems. Wu et al. prepared a series of sulfide catalysts in hydrodeoxygenation of 4-propylguaiacol and the highest selectivity to propylbenzene was observed over CoS_2−MoS_2 at 250 °C.[23] Ohta et al. also studied hydrodeoxygenation of 4-propylphenol over Pt-Re/ZrO_2 and the highest selectivity of *n*-propylbenzene was up to 85% at 2.0 MPa H_2.[24] However, the yield of aromatics was still not satisfactory. Therefore, it is urgent to develop a highly efficient catalyst for the conversion of monophenols into aromatic chemicals and liquid fuels under a low hydrogen pressure.

Niobic acid ($Nb_2O_5 \cdot nH_2O$) as a heterogeneous catalyst with water-tolerant Lewis acid sites was widely used in dehydration[25] and hydrodeoxygenation[17,26,27] processes with favorable results. Nevertheless, the application of Nb_2O_5 in the conversion of lignin and lignin model compounds was still underdeveloped.

Based on the above consideration, a series of Nb_2O_5 with different calcination temperature-supported Rh catalysts were prepared and employed in catalytic hydrodeoxygenation of 2-methoxy-4-propylphenol under a low hydrogen pressure. For comparison, the widely used solid acid catalyst Al_2O_3 was also employed in this work. The effects of the calcination temperature of the support and reaction conditions were discussed in detail. Then, the valorization of lignocellulosic biomass was explored. First, the pine wood was depolymerized into lignin oil in methanol, and then the hydrodeoxygenation of lignin oil was carried out under a low hydrogen pressure.

EXPERIMENTAL SECTION

Catalyst Preparation. $Nb_2O_5 \cdot nH_2O$ was calcined at different temperatures (400, 500, 600, and 700 °C) under an O_2/Ar atmosphere and labeled as Nb_2O_5-400, Nb_2O_5-500, Nb_2O_5-600, and Nb_2O_5-700, respectively.

Rh-supported catalysts were prepared by the incipient wetness method with a certain amount of $RhCl_3 \cdot 3H_2O$ aqueous solution (1.0 g/100 mL) and 1.0 g of the support (Nb_2O_5 and γ-Al_2O_3). The theoretical loading of Rh was kept at 1 wt % for each sample. After impregnation and solvent removal, the as-prepared catalysts were calcined at 400 °C under an O_2/Ar atmosphere for 3 h. All catalysts were reduced at 300 °C under a H_2 atmosphere for 2 h prior to use.

Catalyst Characterization. The loading of Rh was estimated by inductively coupled plasma-optical emission spectroscopy (ICP-OES) with an Optima 2000 DV spectrometer.

The nitrogen adsorption/desorption isotherms were obtained by N_2 physisorption over an Autosorb iQ instrument. The surface area was calculated by the Brunauer−Emmett−Teller (BET) method and the average pore size diameter was determined by the density functional theory (DFT) method.

The dispersion of Rh was determined by carbon monoxide (CO) pulse chemisorption analysis on a Micromeritics Autochem II Chemisorption analyzer. Prior to the test, 50 mg of the sample was placed in a U-shaped quartz tube and reduced under a H_2 atmosphere at 300 °C for 2 h. After that the gas was changed to pure argon and purged until it reached room temperature. Then, CO was introduced and adsorbed repeatedly until the adjacent two peaks had the same CO adsorption peak area.

The X-ray powder diffraction (XRD) patterns were recorded at 40 KV/100 mA with Cu Kα1 radiation (λ = 1.5418 Å) within scattering angles of 5−90°.

Raman spectra were recorded on a Renishaw Raman spectrometer under room temperature in the range of 50−3500 cm^{-1} with the resolution of 2 cm^{-1}, and the wavenumber of the laser source was 532 nm.

The H_2-temperature-programmed reduction (H_2-TPR) profiles were measured with the Micromeritics Autochem II Chemisorption instrument. In a typical run, 50 mg of the catalyst was pretreated in Ar (30 mL/min) at 200 °C for 1 h and then cooled down to ambient temperature. After that, 10 vol % H_2/Ar gas was introduced with a flow rate of 30 mL/min and heated to 700 °C (10 °C/min) using a TCD detector.

NH_3-temperature-programmed desorption (NH_3-TPD) was used to measure the acidity of catalysts. Prior to testing, 100 mg of the sample was pretreated in helium at 450 °C for 1 h and cooled down to 130 °C. After that the sample was saturated with NH_3 for an hour and then flushed with helium to remove all of the physisorbed NH_3. Then, the tested sample was heated from 120 to 550 °C under helium with a 10 °C/min heating rate using a TCD detector.

IR spectra of pyridine were recorded on an EQUIOX-55 infrared spectrometer. Typically, 10 mg of the sample was pretreated at 400 °C for 35 min and cooled down to 50 °C for pyridine adsorption for 5 min. The IR spectrum was recorded after treated at 150 °C for 30 min. The amount of Brønsted and Lewis acid sites were calculated based on the previous report.[28]

Transmission electron microscopy (TEM, FEI Tecnai G2 F30) and high-angle annular detector dark-field scanning transmission electron microscopy (HADDF-STEM) images were obtained to observe the morphology of the supported Rh catalysts and the distribution of the Rh element, respectively.

X-ray photoelectron spectroscopy (XPS) was performed on an ESCALAB XI+ X-ray photoelectron spectrometer produced by Thermo Company. The radiation source was an Al Kα X-ray and the C 1s peak 284.6 eV was applied as a reference for calibrating the binding energy. All samples were prereduced at 300 °C before measurement.

Diffuse reflectance infrared Fourier transform spectra (DRIFTS) were carried out with the Bruker Equinox 55 spectrometer equipped with a mercury cadmium telluride (MCT) detector with a resolution of 4 cm^{-1}. Typically, the sample was reduced at 300 °C for 1 h and purged with helium flow to remove the hydrogen on the surface until cooled down to room temperature. The background was recorded prior to charging with 5% CO/He. After the 5% CO/He was introduced for 5 min, pure He was subsequently introduced to remove physically adsorbed CO, and the spectra were recorded until the spectra were stable.

Thermogravimetric analysis (TGA) of the spent catalyst was conducted over the Discovery SDT 650 model of the TA instrument. During the test, 10 mg of the sample was put into a crucible and heated to 800 °C at a rate of 10 °C/min in air (100 mL/min).

Catalyst Evaluation. *Preparation of Lignin Oil.* Lignin oil was obtained via depolymerization of pine wood based on the literature.[18] Typically, 1.0 g of pine wood powder (dried before use), 0.1 g of 5 wt % Ru/AC (active carbon), and 20 mL of methanol were put into a 50 mL autoclave reactor. The reactor was sealed and purged with hydrogen three times, and the initial 3.0 MPa hydrogen pressure was charged at ambient temperature. The reactor was heated to 220 °C and maintained for 6 h under vigorous stirring. The final pressure in the reactor at the target temperature was 8.5 MPa. After the reactor was cooled down to room temperature, the solid residue (Ru/C and methanol insoluble) was separated and washed with methanol several times by filtration. The methanol was removed from the liquid product by rotary evaporation. After that the obtained residue was extracted with ethyl acetate and water. The lignin oil was mainly concentrated in the ethyl acetate phase, while the aqueous phase mainly contained methylated C_5 sugars.[29] The lignin oil was obtained via removal of ethyl acetate by rotary evaporation. To identify the composition of lignin oil, 5 mL of ethyl acetate was employed to dilute the concentrated lignin oil and *n*-dodecane was used as the internal standard. The specific component of lignin oil was analyzed and determined by gas chromatography−mass spectrometry (GC-MS, Agilent 7890B GC with 5977A MSD). The mass yield of monophenolic compounds in lignin oil were calculated as follows[30,31]

https://dx.doi.org/10.1021/acssuschemeng.0c08478
ACS Sustainable Chem. Eng. 2021, 9, 3529−3541

$$Yx(\text{wt }\%) = \frac{\frac{m_{n-\text{dodecane}}}{170} \times \frac{\frac{A_x}{\text{ECN}(x)}}{A_{n-\text{dodecane}}/12} \times M_x}{m_{\text{lignin}}} \times 100 \quad (1)$$

where m represents the mass (g), A represents the peak area obtained in GC-MS, and M represents the molar mass (g/mol). The effective carbon number (ECN) was used, as described in the literature.[32]

Hydrodeoxygenation of Lignin Oil. Hydrodeoxygenation of lignin oil was carried out in a 50 mL autoclave reactor. Prior to the reaction, the ethyl acetate in the lignin oil solution was removed by rotary evaporation and dried at 80 °C overnight. In a typical run, 50 mg of lignin oil, 0.2 g of *n*-dodecane (internal standard), 20 mL of *n*-decane, and 50 mg of the catalyst were charged into the reactor. After purging with hydrogen three times, 0.5 MPa hydrogen was pressurized (ambient temperature) and the reactor was heated to the desired temperature. The liquid products were identified by GC-MS (Agilent 7890B GC with 5977A MSD) and analyzed by GC (Agilent 7890B). The mass[29] and molar[18] yield of liquid products were calculated as follows

$$Y(\text{wt }\%) = \frac{\text{weight of lignin oil produced}}{\text{weight of pine wood inputted}} \times 100\% \quad (2)$$

$$Yi(\text{mol }\%) = \frac{\text{moles of product } i}{\text{total moles of monophenols in lignin oil}} \times 100\% \quad (3)$$

Hydrodeoxygenation of 2-Methoxy-4-propylphenol. Hydrodeoxygenation (HDO) of the lignin model compound 2-methoxy-4-propylphenol was conducted in a 50 mL autoclave reactor. Typically, 1 mmol substrate, 0.2 g of *n*-dodecane (internal standard), 20 mL of *n*-decane, and 50 mg of the catalyst were added in an autoclave reactor. After the reactor was purged with hydrogen three times, 0.5 MPa hydrogen (ambient temperature) pressure was charged. The reactor was then heated to the desired temperature with a magnetic stirring speed of 700 rpm. After the reaction was completed and cooled down to the ambient temperature, the liquid products were collected and the solids were filtered off before analysis. The composition of liquid products was identified with GC-MS (Agilent 7890B GC with 5977A MSD) and determined by GC (Agilent 7890B). The catalytic performance was evaluated by the conversion of the substrate, selectivity, and yield of the product i, as listed below

$$\text{conversion} = \frac{n^0_{\text{substrate}} - n^f_{\text{substrate}}}{n^0_{\text{substrate}}} \times 100\% \quad (4)$$

$$\text{selectivity}\ (i) = \frac{n_i}{n^0_{\text{substrate}} - n^f_{\text{substrate}}} \times 100\% \quad (5)$$

$$\text{yield}\ (i) = \frac{n_i}{n^0_{\text{substrate}}} \times 100\% \quad (6)$$

RESULTS AND DISCUSSION

Characterization of Catalysts. The content of the metal was estimated by ICP-OES and it was observed that the actual metal loading of all catalysts was close to the theoretical loading of 1 wt %, as presented in Table 1. N_2 physisorption was employed to measure the physical structural properties of pristine supports and catalysts, as listed in Table 1. Obviously, the surface area, total volume, and average pore diameter of supports were all reduced after the introduction of the Rh metal. The specific surface area of the supported Rh catalyst was declined with an increasing calcination temperature of Nb_2O_5, as well as the total pore volume and average pore diameter. Particularly, the specific surface area of Rh/Nb_2O_5 significantly dropped from 107.7 to 45.8 m^2/g when the calcination temperature of Nb_2O_5 was increased from 500 to 600 °C, which indicated that the structure of Nb_2O_5 drastically changed. Figure S1 displayed the N_2 physisorption isotherms and pore size distribution of various samples. All samples exhibited IV-type isotherms with a H3 hysteresis, suggested that all samples were mesoporous materials based on the IUPAC classification. The dispersion of Rh was also evaluated by CO-pulse chemisorption, as presented in Table 1. Clearly, the dispersion of Rh was gradually increased with increasing the calcination temperature of Nb_2O_5, while the dispersion of Rh sharply decreased when the calcination temperature of Nb_2O_5 reached 700 °C, which may be ascribed to the agglomeration of Rh that occurred on the surface of Nb_2O_5-700. For Rh/Nb_2O_5-400, the interface between Rh and Nb_2O_5 was formed after reduction at 300 °C, thus leading to the surface of Rh being covered by NbO_x and the dispersion of Rh declined. The dispersion of Rh gradually increased with the calcination temperature of Nb_2O_5 increasing from 400 to 600 °C, which could result from the reduced coverage of NbO_x on the surface of Rh. Besides, the dispersion of Rh reached 76.6% over the Rh/Al_2O_3 catalyst, which indicated that the preparation method used in this work can ensure that Rh was highly dispersed over the surface of the support.

Table 1. Physical Properties of the Various Catalysts

catalysts	metal loading[a] (wt %)	S_{BET}[b] (m^2/g)	V_{total}[b] (cm^3/g)	D_{pore}[b] (nm)	metal dispersion[c] (%)
Nb_2O_5-400		164.1	0.22	3.5	
Al2O3		213.8	0.46	5.8	
Rh/Nb_2O_5-400	0.96	130.8	0.20	3.4	32.2
Rh/Nb_2O_5-500	0.92	107.7	0.13	3.3	48.2
Rh/Nb_2O_5-600	0.99	45.8	0.10	3.1	55.7
Rh/Nb_2O_5-700	0.87	30.7	0.05	2.6	22.8
Rh/Al_2O_3	0.84	197.2	0.45	5.3	76.6

[a]Determined by ICP-OES. [b]Determined by N_2 adsorption/desorption isotherms and the average pore diameter was determined by the DFT method. [c]CO uptake and metal dispersion were determined by the CO-pulse titration method.

The XRD patterns of various supported Rh catalysts are presented in Figure 1. The diffraction peaks at 2θ = 37.6, 39.4, 45.7, and 66.7° correspond to γ-Al_2O_3 (JCPDS No. 29-0063). The broad diffraction peak at 2θ = 25.3° was assigned to the amorphous Nb_2O_5. It can be seen that the amorphous phase of Nb_2O_5 transformed into the crystalline phase when the calcination temperature exceeded 500 °C, which was consistent with the phenomenon that TT-phase crystallization of Nb_2O_5 was formed at 450 °C.[33] The intensities of diffraction peaks at 2θ = 22.6, 28.3, 36.8, and 46.3° were increased with increasing calcination temperature increased. It should be pointed out that the diffraction peaks located at 26.3, 36.8, 50.7, and 70.9° were divided into two diffraction peaks, which suggested that the orthorhombic structure (T-phase) of Nb_2O_5 (JCPDS #30-0873) was formed when the calcination temperature was increased from 600 to 700 °C.[33,34] In addition, no diffraction peaks ascribed to Rh in all catalysts were observed when compared to XRD patterns of various

https://dx.doi.org/10.1021/acssuschemeng.0c08478
ACS Sustainable Chem. Eng. 2021, 9, 3529−3541

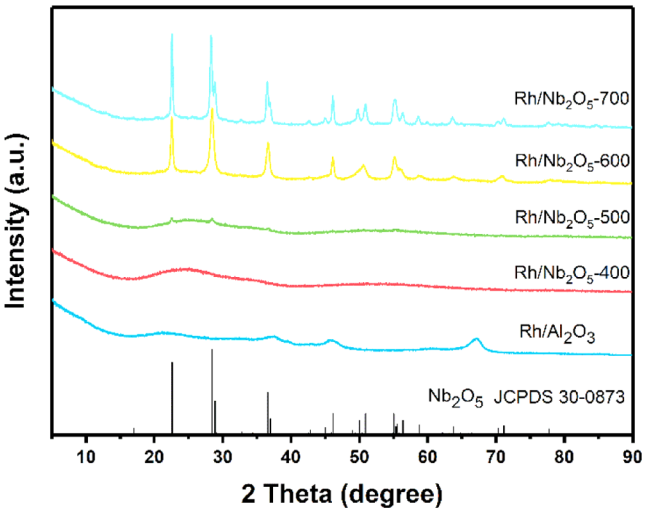

Figure 1. XRD patterns of the supported Rh catalysts.

supports (Figure S2), which may be due to the high dispersion of Rh metal particles over the supports.

Raman spectroscopy is sensitive to the structure and bond order of metal oxides.[35] Herein, the Raman spectra of Nb_2O_5 with different calcination temperature-supported Rh catalysts were investigated to determine the structure of Nb_2O_5, as depicted in Figure 2. The broad asymmetric band in the range

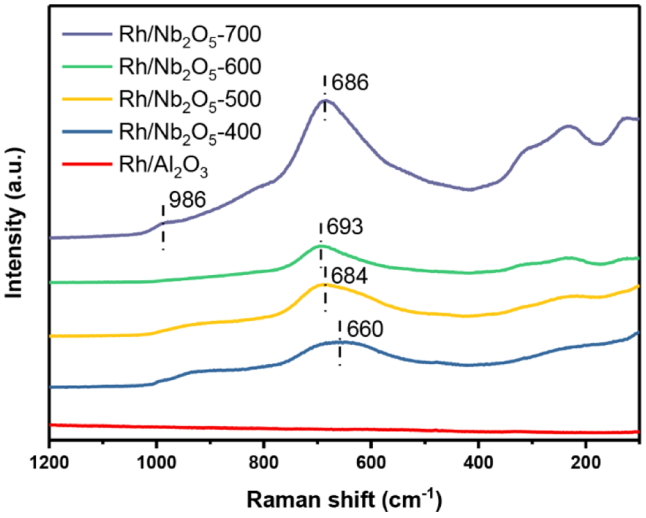

Figure 2. Raman spectra of various supported Rh catalysts.

of 517−768 cm^{-1} was attributed to the stretching mode of the Nb−O polyhedra, including NbO_6, NbO_7, and NbO_8.[17,36] In addition, the peak centered at 660 cm^{-1} was assigned to the Nb−Ob vibrations in amorphous Nb_2O_5 for the Rh/Nb_2O_5-400 sample,[36] which agreed well with XRD results. Compared with Rh/Nb_2O_5-400, the peak position was gradually shifted to a higher wavenumber with the calcination temperature of Nb_2O_5 increased, indicating that the diverse forms of Nb−O polyhedra exhibited some differences on Rh/Nb_2O_5-500 and Rh/Nb_2O_5-600.[17] Moreover, the sharp peak located at 686 cm^{-1} for Rh/Nb_2O_5-700 was correlated to the Nb−O−Nb bridging bond of distorted NbO_6,[37] indicating the presence of T crystal phases.[36] The relative weak band at 986 cm^{-1} was assigned to the stretching vibrations of terminal Nb = O surface groups. Additionally, the Raman bands in the range of 200−400 cm^{-1} were ascribed to the bending vibrations of Nb−O−Nb bonds. For Rh/Al_2O_3, no obvious peak was observed in the range of 100−1200 cm^{-1}.

H_2-TPR was conducted to explore the interaction between Rh and supports, as presented in Figure 3. For Rh/Al_2O_3, a

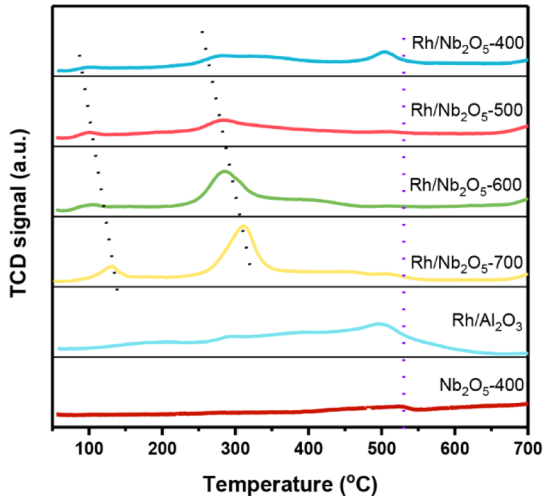

Figure 3. H_2-TPR profiles of the supported Rh catalysts.

weak broad peak between 150 to 250 °C could be ascribed to the reduction of RhO_x species, which has a relative weak interaction with Al_2O_3.[38] The second peak located at around 300 °C was assigned to the strong interaction between RhO_x species and γ-Al_2O_3. In addition, a sharp peak that appeared at 500 °C could be due to the H_2 consumption of surface hydroxyl groups of Al_2O_3.[39] Three reduction peaks were observed for the Rh/Nb_2O_5-400 catalyst, the first peak that appeared at 100 °C corresponded to the reduction of isolated RhO_x, which has a weak interaction with Nb_2O_5-400. The second peak related to the RhO_x species strongly interacted with Nb_2O_5-400. The last peak was assigned to the partial reduction of Nb_2O_5 into NbO_x. Apparently, a broad peak was observed at 280 °C over Rh/Nb_2O_5-400 instead of a sharp peak compared with the other Rh/Nb_2O_5 samples, which could be attributed to the reduction of RhO_x and partially Nb_2O_5. This phenomenon confirmed that the Rh metal could promote the reduction of Nb_2O_5, and there was an interaction between the metal and support as well. To further demonstrate the interaction between Rh and Nb_2O_5, the H_2-TPR of Nb_2O_5-400 was conducted, as shown in Figure 3. It can be seen from Figure 3 that only one weak reduction peak was located at 540 °C for Nb_2O_5-400. After the Rh metal was loaded, the reduction peak shifted to 510 °C and the peak intensity was significantly enhanced, which indicated that there was an interaction between Rh and Nb_2O_5-400. Specifically, the hydrogen dissociated on the surface of the Rh metal to form H radicals and spillover to Nb_2O_5-400, which promoted the partial reduction of the support, thereby forming the NbO_x species. However, with the increase of the calcination temperature of Nb_2O_5, the reduction peaks of RhO_x slightly shifted to higher reduction temperature regions. Meanwhile, the reduction peak of amorphous Nb_2O_5 centered at 510 °C disappeared.

The acid content of supports was evaluated via the NH_3-TPD technique, as shown in Figure 4. A broad NH_3 desorption peak was observed in the testing range between 130 and 550

https://dx.doi.org/10.1021/acssuschemeng.0c08478
ACS Sustainable Chem. Eng. 2021, 9, 3529−3541

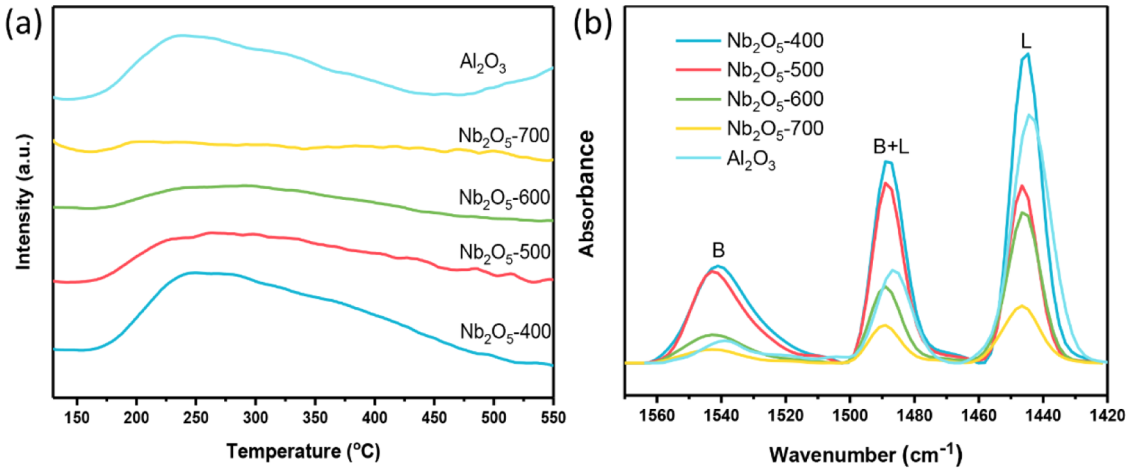

Figure 4. NH_3-TPD (a) and Py-IR (b) profiles of various supports.

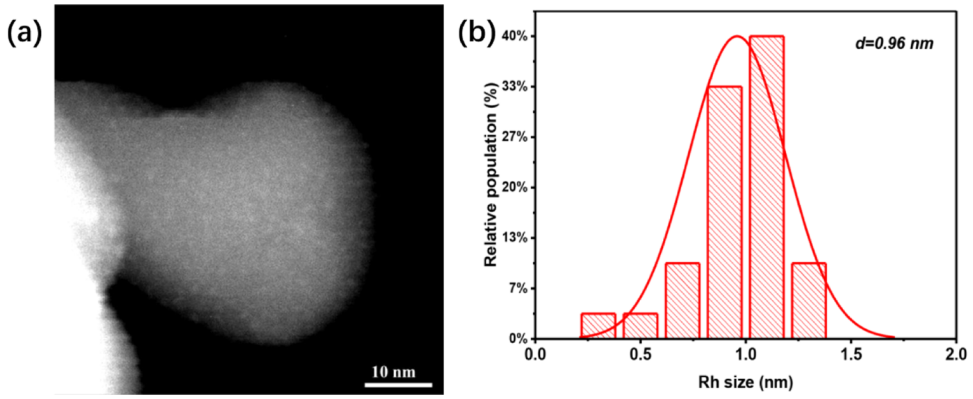

Figure 5. TEM image of (a) reduced Rh/Nb_2O_5-400 and (b) histogram of Rh particle sizes.

°C. For Nb_2O_5, the intensity of the desorption peak gradually decreased with increasing calcination temperature of Nb_2O_5, which illustrated that the total amount of the acid steadily declined. It was worth noting that almost no NH_3 desorption peak was detected for Nb_2O_5-700. The NH_3-TPD profile of Al_2O_3 also showed a broad peak in the range between 175 and 450 °C. To clearly understand the change of the amount of acid content, the concentration of acid sites was determined by the integral of the peak area of various supports, as listed in Table S1. As the calcination temperature extended from 400 to 700 °C, the total content of acid sites decreased from 0.21 mmol NH_3/g cat. to 0.01 mmol NH_3/g cat., indicating that the pretreatment temperature vastly affects the acidic properties of the supports, which agreed well with previous reports.[40,41] Besides, pyridine-Fourier transform infrared (FTIR) was also carried out to evaluate the Lewis and Brønsted acid sites of various supports, as shown in Figure 4b. The amount of Lewis (L) and Brønsted (B) acid sites gradually decreased from 0.17 and 0.11 mmol Py/g cat. to 0.03 and 0.01 mmol Py/g cat. with the calcination temperature of Nb_2O_5 increased from 400 to 700 °C, respectively, as listed in Table S1. These results agreed well with NH_3-TPD results.

The morphology of various reduced Rh/Nb_2O_5 catalysts was investigated with the TEM technique, as shown in Figure S3. It was clearly seen that Nb_2O_5 was gradually transformed from amorphous into the regular morphology with the calcination temperature increasing from 400 to 700 °C. The regular morphology could be observed over Rh/Nb_2O_5-600, which indicated the formation of crystalline Nb_2O_5. As the calcination temperature of Nb_2O_5 extended to 700 °C, the crystal structure was distinctly observed over Rh/Nb_2O_5, which was consistent with XRD results. Most significantly, the presence of Rh was not detected over all Rh/Nb_2O_5 samples on the 100 nm scale (even in 50 nm scale for Rh/Nb_2O_5-400), indicating that Rh metals were highly dispersed over various Nb_2O_5 supports, which agreed well with XRD results that no diffraction peak corresponding to Rh was detected. To further verify our conclusions, the HADDF-STEM image of reduced Rh/Nb_2O_5-400 was obtained on the 10 nm scale, as shown in Figure 5a. The Rh active sites were uniformly dispersed over Nb_2O_5-400, and the average size of the Rh metal was merely 0.96 nm (Figure 5b). This highly dispersed Rh metal was beneficial to improve the utilization of metal active sites.

To elaborate the electronic states of the Rh species, the XPS analysis of various reduced Rh/Nb_2O_5 catalysts in the Rh 3d region was conducted, as presented in Figure 6. The Rh 3d region displayed the spin−orbit splitting doublet peaks of $3d_{5/2}$ and $3d_{3/2}$. The deconvolution of the Rh 3d region exhibited the presence of two pairs of doublets with a theoretical peak area ratio of 60:40. The peaks centered at 307.4 and 312.1 eV were assigned to metallic Rh.[42] Meanwhile, the doublet peaks located at 308.5 and 313.2 eV could be attributed to Rh^{3+}. The relative area of integrated peaks of Rh^0 was 79%, while the peaks of Rh^{3+} merely accounted for 21% over Rh/Nb_2O_5-400, as shown in Table 2. This result indicated that the surface of Rh particles was predominately in the Rh^0 state. Moreover, the

https://dx.doi.org/10.1021/acssuschemeng.0c08478
ACS Sustainable Chem. Eng. 2021, 9, 3529−3541

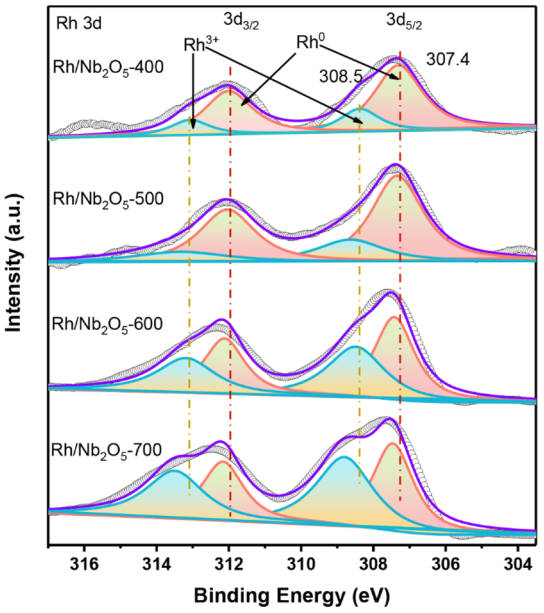

Figure 6. XPS spectra of various Rh/Nb_2O_5 catalysts in the Rh 3d region.

Table 2. Distribution of Different Valence States of Rh 3d as well as the Surface Atomic Ratio of Rh/Nb[a]

	distribution of valence states (%)		
catalysts	Rh^0	Rh^{3+}	surface Rh/Nb ratio
Rh/Nb_2O_5-400	79	21	0.018
Rh/Nb_2O_5-500	74	26	0.037
Rh/Nb_2O_5-600	54	46	0.066
Rh/Nb_2O_5-700	48	52	0.140

[a]As determined by XPS results.

curve fitting of the Rh $3d_{5/2}$ revealed a positive shift of 0.2 eV for the $3d_{5/2}$ peak compared to that of the pure Rh element over Rh/Nb_2O_5-400,[43] which was mainly ascribed to the induced charge on the dispersed Rh particles interacting with Nb_2O_5-400.[44] Additionally, the relative integrated peak areas of Rh^0 were 74, 54, and 48% for Rh/Nb_2O_5-500, Rh/Nb_2O_5-600, and Rh/Nb_2O_5-700, respectively. These results illustrated that with the increasing calcination temperature of Nb_2O_5, the surface content of Rh^0 was gradually reduced. This could be attributed to the enhanced interaction between metal Rh and Nb_2O_5, thus leading to a more difficult situation of the rhodium oxide being reduced, which was consistent with H_2-TPR results. Besides, a pair of peaks were observed at 209.9 and 207.1 eV corresponding to Nb^{5+} in Nb_2O_5,[45] as shown in Figure S4. However, Nb^{4+} was not observed in the XPS result over the reduced Rh/Nb_2O_5-400 sample, which might be ascribed to the fact that only a small part of the surface Nb_2O_5 was reduced into NbO_x. Simultaneously, the surface Rh/Nb ratio gradually increased with increasing the calcination temperature of Nb_2O_5, indicating that the Rh metal was progressively enriched on the surface of the catalyst, as listed in Table 2. This result illustrated that Rh was partially covered by NbO_x due to the existence of the metal−support interaction, resulting in a decreased surface content of the exposed Rh metal.

CO-DRIFTS were employed to explore the adsorption site Rh species over various reduced Rh/Nb_2O_5 catalysts, as shown in Figure 7. For all samples, three CO adsorption peaks were observed in the range of 1950−2150 cm^{-1}. The peak centered

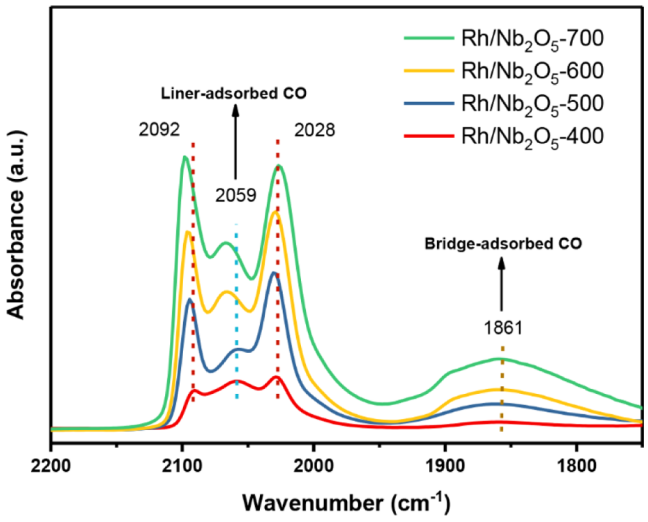

Figure 7. CO-DRIFTS spectra of reduced Rh/Nb_2O_5 catalysts.

at 2059 cm^{-1} was assigned to the adsorption of CO on the metallic Rh species.[46,47] Besides, two peaks that appeared at around 2028 and 2092 cm^{-1} were ascribed to the symmetric and asymmetric stretching vibrations of geminal dicarbonyl species of $Rh(CO)_2$, similar results were also observed over Rh/TiO_2[48] and Rh/ZrO_2,[49] which uniquely existed at Rh-isolated sites over the Nb_2O_5 surface.[48] The intensity of these two peaks gradually increased with the increasing calcination temperature of Nb_2O_5, while the relative intensity of the peak located at 2059 cm^{-1} declined. This phenomenon indicated that the relative concentration of metallic Rh gradually decreased with the calcination temperature of Nb_2O_5 increasing from 400 to 700 °C, which agreed well with XPS results. Interestingly, the CO adsorption peak that appeared at 1861 cm^{-1} (bridge-adsorbed CO) was absent over Rh/Nb_2O_5-400, while the intensity of this peak constantly increased with the increasing calcination temperature of Nb_2O_5. Based on the previous reports, the peak centered at 1861 cm^{-1} was attributed to the Rh nanoparticle sites.[47,49] However, no obvious Rh diffraction peaks were observed in all supported Rh catalysts based on the XRD results. Hence, the bridge-adsorbed CO peak at 1861 cm^{-1} should be attributed to the presence of small Rh clusters or nanoparticles. Therefore, the Rh clusters or nanoparticles were formed when the calcination temperature of Nb_2O_5 was beyond 500 °C. These results obtained in CO-DRIFTS indicated that the calcination temperature of Nb_2O_5 played a vital role in the dispersion of Rh. The atomically dispersed Rh existed over the surface of Nb_2O_5-400, while the small Rh clusters or nanoparticles emerged with the elevated calcination temperature of Nb_2O_5. Therefore, all of these results obtained in various characterizations illustrated that the calcination temperature has a critical influence on the structure of catalysts.

Catalytic Hydrodeoxygenation of 2-Methoxy-4-propylphenol. *Catalyst Screening.* The catalytic performance of supported Rh catalysts was screened via the hydrodeoxygenation of the representative lignin phenolic model compound 2-methoxy-4-propylphenol at 260 °C and 0.1 MPa hydrogen pressure for 4 h, as shown in Figure 8. Obviously, the yield of the oxygen-free propylbenzene product gradually decreased

https://dx.doi.org/10.1021/acssuschemeng.0c08478
ACS Sustainable Chem. Eng. 2021, 9, 3529−3541

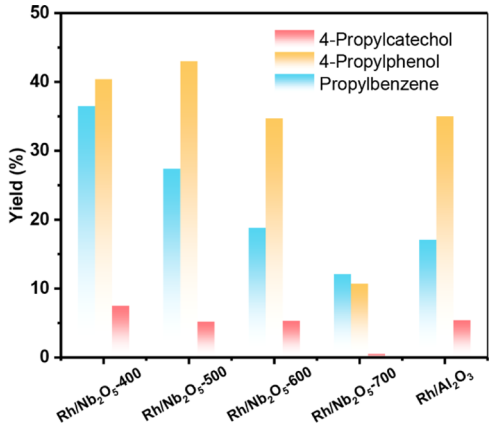

Figure 8. Catalytic hydrodeoxygenation of 2-methoxy-4-propylphenol over various catalysts. Reaction conditions: 260 °C, 0.1 MPa H_2 pressure (ambient temperature), 4 h, 0.05 g of the catalyst, 1 mmol substrate, and 700 rpm.

from 36.5 to 12.1% with the calcination temperature of Nb_2O_5 increased from 400 to 700 °C. From the point of view of acidity, it was found that with increasing total acidic site concentration, the conversion and the capacity of breaking of C−O bonds increased, leading to the boosted yield of the oxygen-free product propylbenzene. Although the total acid content of Nb_2O_5 gradually decreased with raising the calcination temperature of the support, the yields of oxygen-containing products (4-propylphenol and 4-propylcatechol) among the other three Nb_2O_5-supported catalysts were similar except for the Rh/Nb_2O_5-700 catalyst. This phenomenon indicated that the change of acidity of supports was not the only reason for the different catalytic performance over Rh/Nb_2O_5 catalysts. Herein, we speculated that the metal active sites also affected the catalytic performance of HDO of 2-methoxy-4-propylphenol. This could be ascribed to the fact that the surface content of Rh^0 gradually decreased with increasing calcination temperature of Nb_2O_5, as confirmed in XPS and CO-DRIFTS results. Thus, the Rh/Nb_2O_5-400 catalyst could provide more metallic Rh active sites and then promote the dissociation of molecular hydrogen into active H atoms. Subsequently, the H atoms were a spillover from metallic Rh to the surface of Nb_2O_5, which promoted the formation of NbO_x at the metal−support interface. In addition, the atomically dispersed Rh gradually transformed into small Rh clusters or nanoparticles with the increasing calcination temperature of Nb_2O_5, thus leading to the reduction of metal active sites, as confirmed by CO-DRIFTS results. Besides, the CO-pulse chemisorption measurement further demonstrated the formation of the interface between Rh and Nb_2O_5, especially for the Rh/Nb_2O_5-400 catalyst. Consequently, the best result obtained over Rh/Nb_2O_5-400 was attributed to the cooperation between the atomically dispersed Rh metal and NbO_x, in which Rh was responsible for hydrogen dissociation and NbO_x for cleavage of C−O bonds. Although Rh/Al_2O_3 has suitable acidity and high dispersion of Rh, the yield of propylbenzene obtained over Rh/Al_2O_3 (17.1%) was lower than that achieved over the Rh/Nb_2O_5-400 (36.5%) catalyst, which could be attributed to the interaction between Rh and Al_2O_3, which was weaker than Rh and Nb_2O_5-400, as confirmed by H_2-TPR results. As a result, Rh/Nb_2O_5-400 was selected as the target catalyst in the following study.

Optimization of Reaction Conditions. Although the Rh/Nb_2O_5-400 catalyst exhibited favorable results, the yield of propylbenzene was still not satisfactory. Therefore, further experiments including the effects of reaction temperature, hydrogen pressure, and reaction time were conducted to obtain the best results under the optimized reaction conditions.

Reaction performance as a function of the hydrogen pressure was discussed at the beginning, as presented in Table 3. The yield of propylcyclohexane significantly increased with the hydrogen pressure raised and reached 100% under 2.0 MPa hydrogen pressure, while the yield of the oxygen-containing product 4-propylphenol sharply decreased. This result demonstrated that sufficient hydrogen facilitated the aromatic saturation and promoted the cleavage of C−O bonds. The highest yield of propylbenzene (98.0%) was obtained under 0.5 MPa hydrogen pressure. Therefore, the 0.5 MPa hydrogen pressure was identified as the most suitable reaction pressure for the achieving the highest yield of aromatics.

The reaction temperature was also evaluated at 4 h for 0.5 MPa hydrogen pressure in the temperature range of 200−260 °C, as listed in Table 3. The yield of propylcyclohexane decreased along with increasing reaction temperature, while the yield of propylbenzene increased. The highest yield of propylbenzene was achieved at 260 °C; thus, the optimized reaction temperature was fixed at 260 °C.

After the optimized reaction hydrogen pressure and reaction temperature, the best reaction time was also explored to give

Table 3. Optimization of Reaction Conditions over Rh/Nb_2O_5-400[a]

	reaction conditions			yield (%)			
entry	temperature (°C)	time (h)	pressure (MPa)	propylcyclohexane	propylbenzene	4-propylphenol	4-propylcatechol
1	260	4	0.1	0	36.5	40.4	7.5
2	260	4	0.5	2.0	98.0	0	0
3	260	4	1.0	35.0	65.0	0	0
4	260	4	2.0	100	0	0	0
5	200	4	0.5	10.2	40.3	8.1	1.7
6	220	4	0.5	8.7	57.0	12.5	0
7	240	4	0.5	2.6	80.1	11.9	0
8	260	0.5	0.5	0	21.9	18.9	0.5
9	260	1.0	0.5	0	35.6	31.6	2.8
10	260	2.0	0.5	2.7	87.4	4.7	0
11	260	3.0	0.5	3.6	90.1	2.3	0.5

[a]Reaction conditions: 0.05 g of the catalyst, 1 mmol 2-methoxy-4-propylphenol, and 700 rpm.

https://dx.doi.org/10.1021/acssuschemeng.0c08478
ACS Sustainable Chem. Eng. 2021, 9, 3529−3541

Scheme 1. Proposed Reaction Pathway for Hydrodeoxygenation of 2-Methoxy-4-Propylphenol over Rh/Nb_2O_5-400

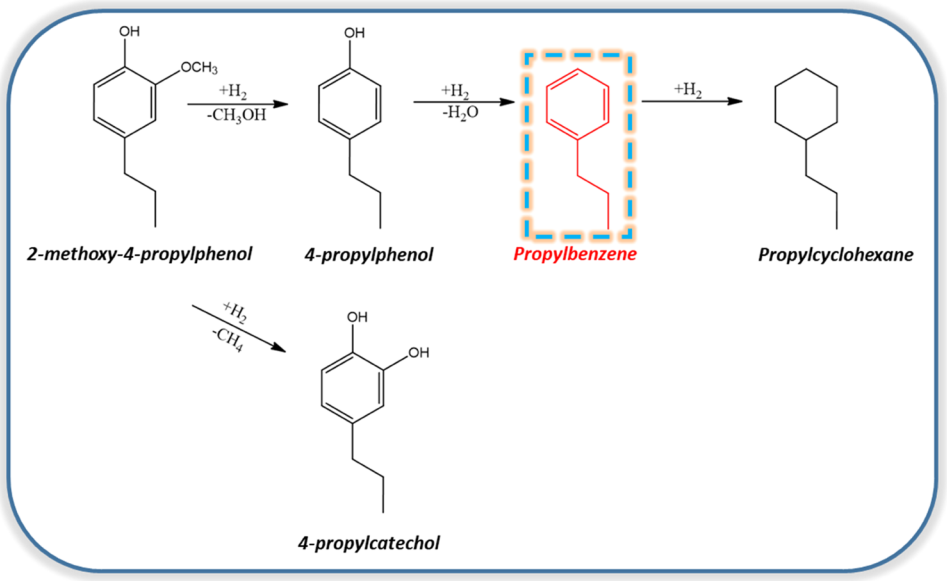

Table 4. Catalytic Hydrodeoxygenation of Lignin-Derived Monophenols over Rh/Nb_2O_5-400[a]

Substrates	Conversion (%)	Main Product	Selectivity (%)
	>99		>99
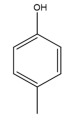	>99		>99
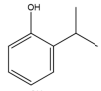	>99	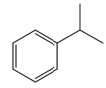	>99
	>98		>99
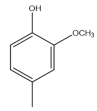	>99		>99
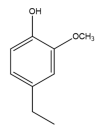	>99	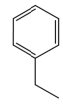	>99
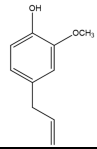	>99	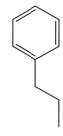	>97

[a]Reaction conditions: 260 °C, 0.5 MPa H_2 pressure (ambient temperature), 4 h, 0.05 g of the catalyst, 1 mmol substrate, and 700 rpm.

an insight of the reaction pathway, as presented in Table 3. Obviously, propylcyclohexane was not detected within 1 h. The yield of propylbenzene significantly grew from 21.9 to 98.0% with the reaction time increased from 0.5 to 4 h, as listed in Table 3. However, the yield of 4-propylphenol increased at the beginning and then declined with prolonged reaction time, indicating that 4-propylbenzene was the initial product in this reaction system. Moreover, a trace of 4-propylcatechol was detected, which could have resulted from the alkylation of 2-methoxy-4-propylphenol. It should be noted that the side reaction product was only observed at a low hydrogen pressure, low temperature, and short reaction time.

https://dx.doi.org/10.1021/acssuschemeng.0c08478
ACS Sustainable Chem. Eng. 2021, 9, 3529−3541

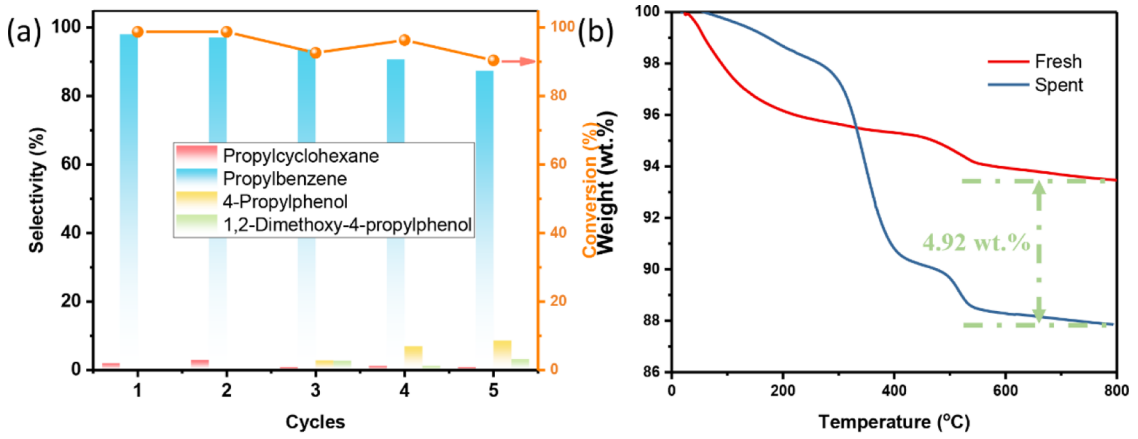

Figure 9. (a) Stability tests for hydrodexoygenation of 2-methoxy-4-propylphenol over Rh/Nb_2O_5-400 and (b) TG profiles of the fresh and spent Rh/Nb_2O_5-400 catalyst. Reaction conditions: 260 °C, 0.5 MPa H_2 pressure (ambient temperature), 4 h, 0.05 g of the catalyst, 1 mmol substrate, and 700 rpm.

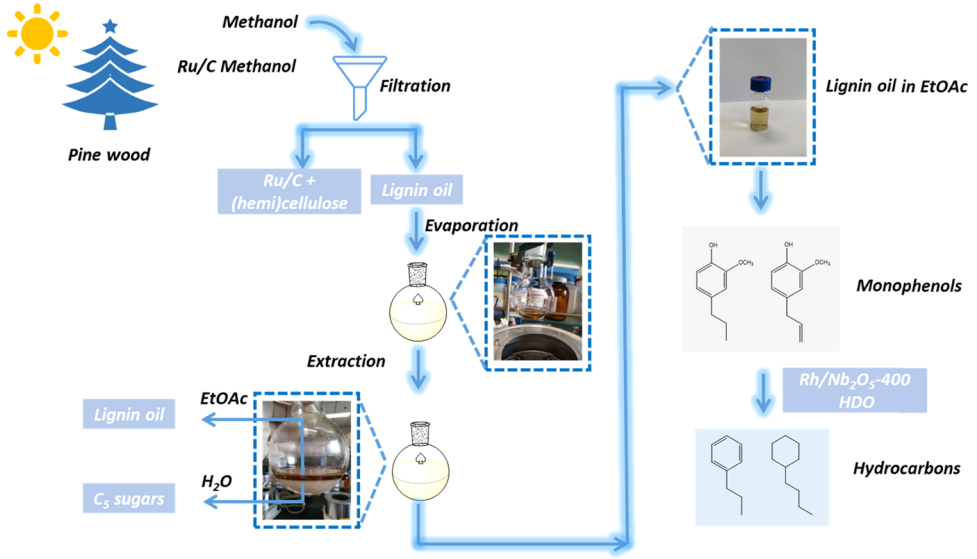

Figure 10. Schematic for valorization of pine wood lignocellulose into hydrocarbons.

Therefore, to avoid the formation of byproducts and ensure the maximum yield of propylbenzene, the optimal reaction conditions were 260 °C and 0.5 MPa hydrogen pressure for 4 h.

Based on the above discussion, the possible reaction pathway was proposed, as shown in Scheme 1. 2-Methoxy-4-propylphenol was first attached to the surface of the catalyst through adsorption and the interaction with Nb_2O_5. Meanwhile, H_2 was adsorbed and dissociated over Rh^0 to produce active H atoms. Then, the oxygen atoms of the methoxy groups were removed by the cooperation of active H atoms and acid sites, thus leading to the formation of methanol and 4-propylphenol. The demethoxylation of 2-methoxy-4-propylphenol into 4-propylphenol was dominant at the beginning of the reaction, which was in agreement with the fact that the bond dissociation of C_{sp2}−OH (466 kJ/mol) was higher than that of C_{sp3}−OMe (409−421 kJ/mol).[50] Thus, the primary product was 4-propylphenol instead of *o*-propylanisole. Meanwhile, a trace amount of 4-propylcatechol was formed through the demethylation/hydrogenation of 2-methoxy-4-propylphenol. The propylbenzene was obtained via the hydrogenolysis of 4-propylphenol. Besides, a small amount of propylbenzene was further hydrogenated to produce propylcyclohexane.

Hydrodeoxygenation of Other Lignin Monophenols. A great number of phenolic compounds were produced during the depolymerization of lignin, such as phenol, guaiacol, p-cresol, 4-ethyl-2-methoxyphenol, etc. Since excellent results were achieved in catalytic hydrodeoxygenation of 2-methoxy-4-propylphenol over the Rh/Nb_2O_5-400 catalyst, we also investigated the catalytic performance of other lignin-derived phenols, as listed in Table 4. Encouragingly, all monophenolic compounds were almost completely converted over Rh/Nb_2O_5-400 at 260 °C and 0.5 MPa H_2. At the same time, the main product was aromatic and the selectivity of aromatics was close to 100%. These results were inspiring and confirmed that Rh/Nb_2O_5-400 was a highly efficient catalyst for breaking C−O bonds to produce aromatic products, which also indicated that Rh/Nb_2O_5-400 was a promising candidate catalyst for valorization of lignin bio-oil into valuable aromatics.

Stability Tests. The reusability of Rh/Nb_2O_5-400 was evaluated under the optimal reaction conditions, as presented in Figure 9a. The conversion of 2-methoxy-4-propylphenol

https://dx.doi.org/10.1021/acssuschemeng.0c08478
ACS Sustainable Chem. Eng. 2021, 9, 3529−3541

slightly declined from 98.7 to 90.4% after 5 cycles. Meanwhile, the selectivity to propylbenzene decreased by 10% after 5 runs, while the oxygen-containing product 4-propylphenol appeared at the third cycle and then the concentration of 4-propylphenol gradually increased. A similar phenomenon was also observed in our previous report.[51] The TG analysis was introduced to examine the carbon deposition of the spent Rh/Nb_2O_5-400 catalyst after 5 cycles, as shown in Figure 9b. The weight of the fresh catalyst was decreased by 6.54 wt % at 800 °C under air, which was mainly attributed to the removal of H_2O in Nb_2O_5. Meanwhile, the sharp decline observed at around 500 °C indicated the transformation of amorphous Nb_2O_5 into crystalline Nb_2O_5, which was consistent with the XRD result. For the spent Rh/Nb_2O_5-400 catalyst after 5 cycles, the total weight loss reached 11.46 wt %, indicating that the coke formation occurred and accounted for 4.92 wt %. Hence, a part of active sites was occupied by carbon deposition, resulting in the decline of catalytic conversion. Simultaneously, the acidity of Nb_2O_5 decreased after stability tests, thus leading to the decline of selectivity of propylbenzene, which we have confirmed in our previous report.[51]

Catalytic Hydrodeoxygenation of Lignin Bio-Oils. *Reductive Depolymerization of Lignocellulosic Biomass.* Inspired by the good results obtained in the catalytic hydrodeoxygenation of 2-methoxy-4-propylphenol and considering that the lignin oil produced by the depolymerization of lignocellulose contains many phenolic compounds, the catalytic upgrading of lignin oil was also explored over Rh/Nb_2O_5-400. Herein, we proposed a two-step process for valorization of lignocellulose into valuable hydrocarbons. The first step involved reductive depolymerization of pine wood over Ru/C in methanol solution. The total schematic for transformation of pine wood into aromatics is shown in Figure 10. The obtained liquid products were analyzed by the GPC technique, as shown in Figure S5. The number-average molecular weight (M_n), weight-average molecular weight (M_w), and polydispersity (M_w/M_n) were 273, 416, and 1.52 g/mol, respectively. The GPC results demonstrated that pine wood was successfully depolymerized into small fraction molecules.

To further understand the structure and functional groups of lignin oil, FTIR was used for the analysis of lignin oil, as shown in Figure 11. Obviously, the peaks at 1031 and 1270 cm^{-1} were assigned to the C−O stretching in the $-OCH_3$ group.[52] In addition, the peaks located at 1462,1514, and 1602 cm^{-1} were attributed to the C═C stretching in aromatics.[53] A sharp peak at 1720 cm^{-1} was ascribed to the C═O stretching in aldehydes or ketones. Moreover, the intense peak at 2870 cm^{-1} could be assigned to the C−H stretching in the aldehyde group. Another peak centered at 2935 cm^{-1} could be ascribed to the C−H stretching in alkyl groups. Besides, a broad peak at 3416 cm^{-1} was assigned to the hydroxyl group. In summary, several oxygen functional groups including $-OCH_3$, −OH, and −CHO were identified in lignin oil. Meanwhile, the benzene ring was also observed, which indicated that the aromatic structure remained well. These results also demonstrated that the lignocellulose was depolymerized into small molecule fragments.

To clearly understand the composition of lignin oil, the GC-MS technique was introduced, as shown in Figure S6b. The lignin oil was diluted in ethyl acetate (EtOAc) before the GC-MS analysis and the liquid lignin oil appeared bright yellow. Apparently, the main products of lignin oil were monophenols,

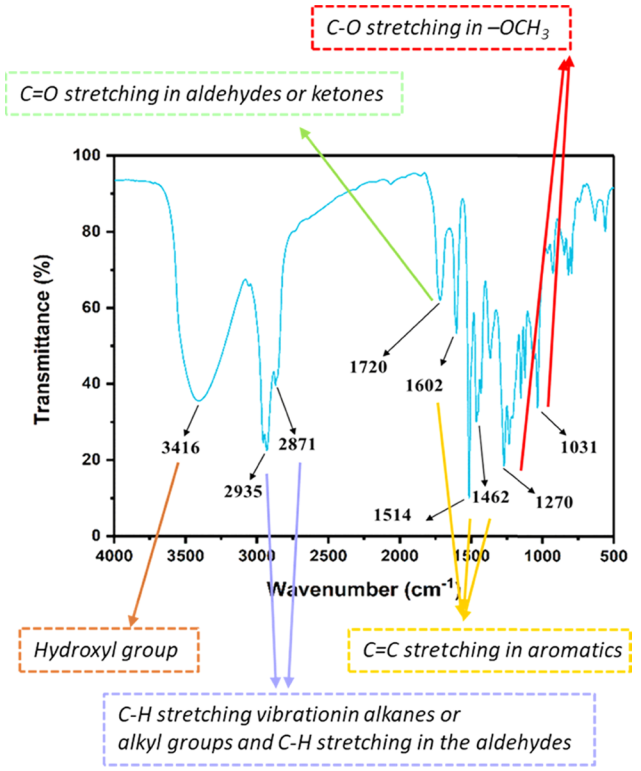

Figure 11. FTI R spectra of lignin oil.

such as 4-propylphenol, 2-methoxy-4-ethylphenol, 2-methoxy-4-propylphenol, eugenol, etc. Among all monophenols, 2-methoxy-4-propylphenol was the most abundant liquid product. Besides, only one dimer phenol was detected, which was 4-phenylphenol. The total mass yield of monophenolic compounds was up to 9.1 wt % yield of pine wood after reductive catalytic depolymerization, in which 76.0% selectivity (moles of product i/total moles of products in lignin oil) of lignin monomer was 2-methoxy-4-propylphenol. Hence, Ru/C was an efficient catalyst for depolymerization of lignocellulose into monophenols. This was mainly because Ru/C could rapidly stabilize the intermediates, hence restrained the polymerization of monophenols to oligomers.[18] Apart from monophenols, 4-methylphenylbutyraldehyde was also observed. These detected liquid products agreed well with the FTIR results.

Catalytic Hydrodeoxygenation of Lignin Oil. Good results were achieved in the catalytic hydrodeoxygenation of 2-methoxy-4-propylphenol; therefore, the catalytic performance of hydrodeoxygenation of lignin oil was also carried out over Rh/Nb_2O_5-400 under the same reaction conditions in the second step. The obtained liquid products were identified with GC-MS, as shown in Figure S6a. Clearly, almost all of the lignin oil was completely converted into liquid products. More significantly, the liquid products were composed of C_6-C_{10} hydrocarbons without oxygen-containing products after the reaction (selectivity > 99%). The liquid products that included toluene, ethylbenzene, propylcyclohexane, propylbenzene, etc. could be obtained via the complex reaction pathways, such as transalkylation, hydrodeoxygenation, etc. The molar yield of liquid products is listed in Table 5, and most of them are aromatic compounds and the total molar yield of aromatic compounds is up to 80.1 mol %. These results confirmed that lignin oil could be transformed into aromatics over Rh/Nb_2O_5-

https://dx.doi.org/10.1021/acssuschemeng.0c08478
ACS Sustainable Chem. Eng. 2021, 9, 3529−3541

Table 5. Catalytic Hydrodeoxygenation of Lignin Oil over Rh/Nb_2O_5[a]

products	products distribution (mol %)
toluene	1.9
ethylbenzene	1.9
propylcyclohexane	7.3
propylbenzene	30.5
4-ethyltoluene	37.6
butylcyclohexane	12.6
4-propyltoluene	8.2

[a]Reaction conditions: 260 °C, 0.5 MPa H_2, 4 h, 0.05 g of Rh/Nb_2O_5-400, 0.05 g of lignin oil, and 700 rpm.

400, indicating that Rh/Nb_2O_5-400 was a promising catalyst for cleavage of C−O in lignin phenolic compounds. Meanwhile, the results also confirmed that the two-step method for valorization of biomass into valuable hydrocarbons was available.

CONCLUSIONS

The catalytic hydrodeoxygenation of the lignin monophenolic model compound 2-methoxy-4-propylphenol was investigated over various supported Rh catalysts. The highest yield of propylbenzene (98%) was obtained over Rh/Nb_2O_5-400 under 0.5 MPa H_2. In addition, the other lignin-derived monophenols were also nearly quantitatively converted into aromatics over Rh/Nb_2O_5-400 with selectivity of aromatics > 97% under the same reaction conditions. More significantly, the two steps for conversion of lignocellulosic biomass into hydrocarbons was also carried out. First, pine wood was depolymerized into lignin oil over Ru/C in methanol with a 9.1 wt % mass yield of monophenols, and the selectivity of 2-methoxy-4-propylphenol reached 76% in lignin oil. After that, the catalytic hydrodeoxygenation of lignin oil was carried out over Rh/Nb_2O_5-400 under 0.5 MPa H_2. All liquid products were composed of C_6−C_{10} hydrocarbons with >99% selectivity and 80.1 mol % yield of them were aromatics. All results obtained in this work shed light on the fact that valorization of lignocellulosic biomass was a promising method to produce aromatics.

ASSOCIATED CONTENT

Supporting Information

The Supporting Information is available free of charge at https://pubs.acs.org/doi/10.1021/acssuschemeng.0c08478.

N_2 physical sorption isotherms (Figure S1); XRD patterns of the various supports (Figure S2); acidic properties of different supports (Table S1); TEM images of various Rh/Nb_2O_5 catalysts (Figure S3); Nb 3d photoemission spectra (Figure S4); GPC curve of lignin oil (Figure S5); and GC-MS spectrum of lignin oil and lignin oil products (Figure S6) (PDF)

AUTHOR INFORMATION

Corresponding Author

Changhai Liang − *State Key Laboratory of Fine Chemicals, Laboratory of Advanced Materials and Catalytic Engineering, School of Chemical Engineering, Dalian University of Technology, Dalian 116024, China;* orcid.org/0000-0001-7959-251X; Email: changhai@dlut.edu.cn

Authors

Weixiang Guan − *State Key Laboratory of Fine Chemicals, Laboratory of Advanced Materials and Catalytic Engineering, School of Chemical Engineering, Dalian University of Technology, Dalian 116024, China*

Xiao Chen − *State Key Laboratory of Fine Chemicals, Laboratory of Advanced Materials and Catalytic Engineering, School of Chemical Engineering, Dalian University of Technology, Dalian 116024, China*

Chi Wing Tsang − *Faculty of Science and Technology, Technological and Higher Education Institute of Hong Kong, Hong Kong, China*

Haoquan Hu − *State Key Laboratory of Fine Chemicals, Laboratory of Advanced Materials and Catalytic Engineering, School of Chemical Engineering, Dalian University of Technology, Dalian 116024, China;* orcid.org/0000-0002-5288-2186

Complete contact information is available at: https://pubs.acs.org/10.1021/acssuschemeng.0c08478

Notes

The authors declare no competing financial interest.

ACKNOWLEDGMENTS

This work was supported by the National Key Research and Development Program of China (2016YFB0600305) and the Research Grants Council of the Hong Kong Special Administrative Region, China (UGC/FDS25/E09/17).

REFERENCES

(1) Li, C.; Zhao, X.; Wang, A.; Huber, G. W.; Zhang, T. Catalytic transformation of lignin for the production of chemicals and fuels. *Chem Rev.* **2015**, *115*, 11559−11624.

(2) Wu, Z.; Zhao, X.; Zhang, J.; Li, X.; Zhang, Y.; Wang, F. Ethanol/1,4-dioxane/formic acid as synergistic solvents for the conversion of lignin into high-value added phenolic monomers. *Bioresour. Technol.* **2019**, *278*, 187−194.

(3) Dutta, S.; De, S.; Saha, B.; Alam, M. I. Advances in conversion of hemicellulosic biomass to furfural and upgrading to biofuels. *Catal. Sci. Technol.* **2012**, *2*, 2025−2036.

(4) Ruppert, A. M.; Weinberg, K.; Palkovits, R. Hydrogenolysis Goes Bio: From carbohydrates and sugar alcohols to platform chemicals. *Angew. Chem., Int. Ed.* **2012**, *51*, 2564−2601.

(5) Rautiainen, S.; Di Francesco, D.; Katea, S. N.; Westin, G.; Tungasmita, D. N.; Samec, J. S. M. Lignin valorization by cobalt-catalyzed fractionation of lignocellulose to yield monophenolic compounds. *ChemSusChem* **2019**, *12*, 404−408.

(6) Ouyang, X.; Huang, X.; Zhu, J.; Boot, M. D.; Hensen, E. J. M. Catalytic conversion of lignin in woody biomass into phenolic monomers in methanol/water mixtures without external hydrogen. *ACS Sustainable Chem. Eng.* **2019**, *7*, 13764−13773.

(7) Jiang, Z.; Hu, C. Selective extraction and conversion of lignin in actual biomass to monophenols: A review. *J. Energy Chem.* **2016**, *25*, 947−956.

(8) Wang, H.; Ben, H.; Ruan, H.; Zhang, L.; Pu, Y.; Feng, M.; Ragauskas, A. J.; Yang, B. Effects of lignin structure on hydrodeoxygenation reactivity of pine wood lignin to valuable chemicals. *ACS Sustainable Chem. Eng.* **2017**, *5*, 1824−1830.

(9) Chen, Q.; Cai, C.; Zhang, X.; Zhang, Q.; Chen, L.; Li, Y.; Wang, C.; Ma, L. Amorphous FeNi−ZrO_2-catalyzed hydrodeoxygenation of lignin-derived phenolic compounds to naphthenic fuel. *ACS Sustainable Chem. Eng.* **2020**, *8*, 9335−9345.

(10) Tieuli, S.; Mäki-Arvela, P.; Peurla, M.; Eränen, K.; Wärnå, J.; Cruciani, G.; Menegazzo, F.; Murzin, D. Y.; Signoretto, M. Hydrodeoxygenation of isoeugenol over Ni-SBA-15: Kinetics and modelling. *Appl. Catal., A* **2019**, *580*, 1−10.

(11) de Souza, P. M.; Rabelo-Neto, R. C.; Borges, L. E. P.; Jacobs, G.; Davis, B. H.; Resasco, D. E.; Noronha, F. B. Hydrodeoxygenation of phenol over Pd catalysts. effect of support on reaction mechanism and catalyst deactivation. *ACS Catal.* **2017**, *7*, 2058−2073.
(12) Zhang, X.; Tang, W.; Zhang, Q.; Wang, T.; Ma, L. Hydrodeoxygenation of lignin-derived phenoic compounds to hydrocarbon fuel over supported Ni-based catalysts. *Appl. Energy* **2018**, *227*, 73−79.
(13) Cao, Z.; Engelhardt, J.; Dierks, M.; Clough, M. T.; Wang, G. H.; Heracleous, E.; Lappas, A.; Rinaldi, R.; Schuth, F. Catalysis meets nonthermal separation for the production of (alkyl)phenols and hydrocarbons from pyrolysis oil. *Angew. Chem., Int. Ed.* **2017**, *56*, 2334−2339.
(14) Gao, D.; Schweitzer, C.; Hwang, H. T.; Varma, A. Conversion of guaiacol on noble metal catalysts: Reaction performance and deactivation studies. *Ind. Eng. Chem. Res.* **2014**, *53*, 18658−18667.
(15) Resasco, J.; Yang, F.; Mou, T.; Wang, B.; Christopher, P.; Resasco, D. E. Relationship between atomic scale structure and reactivity of Pt catalysts: Hydrodeoxygenation of m-cresol over isolated pt cations and clusters. *ACS Catal.* **2020**, *10*, 595−603.
(16) Wang, W.; Zhang, K.; Li, L.; Wu, K.; Liu, P.; Yang, Y. Synthesis of highly active Co−Mo−S unsupported catalysts by a one-step hydrothermal method for p-cresol hydrodeoxygenation. *Ind. Eng. Chem. Res.* **2014**, *53*, 19001−19009.
(17) Xin, Y.; Dong, L.; Guo, Y.; Liu, X.; Hu, Y.; Wang, Y. Correlation of the catalytic performance with Nb_2O_5 surface properties in the hydrodeoxygenation of lignin model compound. *J. Catal.* **2019**, *375*, 202−212.
(18) Liu, X.; Wang, C.; Zhang, Y.; Qiao, Y.; Pan, Y.; Ma, L. Selective preparation of 4-alkylphenol from lignin-derived phenols and raw biomass over magnetic Co-Fe@N-Doped carbon catalysts. *ChemSusChem* **2019**, *12*, 4791−4798.
(19) Gao, X.; Zhu, S.; Li, Y. Selective hydrogenolysis of lignin and model compounds to monophenols over AuPd/CeO_2. *Mol. Catal.* **2019**, *462*, 69−76.
(20) Song, S.; Zhang, J.; Yan, N. Support effects in the demethoxylation of lignin monomer 4-propylguaiacol over molybdenum-based catalysts. *Fuel Process. Technol.* **2020**, *199*, 106224−106231.
(21) Yohe, S. L.; Choudhari, H. J.; Mehta, D. D.; Dietrich, P. J.; Detwiler, M. D.; Akatay, C. M.; Stach, E. A.; Miller, J. T.; Delgass, W. N.; Agrawal, R.; Ribeiro, F. H. High-pressure vapor-phase hydrodeoxygenation of lignin-derived oxygenates to hydrocarbons by a PtMo bimetallic catalyst: Product selectivity, reaction pathway, and structural characterization. *J. Catal.* **2016**, *344*, 535−552.
(22) Hossain, M. A.; Phung, T. K.; Rahaman, M. S.; Tulaphol, S.; Jasinski, J. B.; Sathitsuksanoh, N. Catalytic cleavage of the β-O-4 aryl ether bonds of lignin model compounds by Ru/C catalyst. *Appl. Catal., A* **2019**, *582*, 117100−117106.
(23) Wu, K.; Liu, Y.; Wang, W.; Huang, Y.; Li, W.; Shi, Q.; Yang, Y. Preparation of hydrophobic MoS_2, NiS_2-MoS_2 and CoS_2-MoS_2 for catalytic hydrodeoxygenation of lignin-derived phenols. *Mol. Catal.* **2019**, *477*, 110537−110544.
(24) Ohta, H.; Feng, B.; Kobayashi, H.; Hara, K.; Fukuoka, A. Selective hydrodeoxygenation of lignin-related 4-propylphenol into n-propylbenzene in water by Pt-Re/ZrO_2 catalysts. *Catal. Today* **2014**, *234*, 139−144.
(25) Nakajima, K.; Baba, Y.; Noma, R.; Kitano, M.; Kondo, J. N.; Hayashi, S.; Hara, M. Nb_2O_5·nH_2O as a heterogeneous catalyst with water-tolerant Lewis acid sites. *J. Am. Chem. Soc.* **2011**, *133*, 4224−4227.
(26) Leal, G. F.; Lima, S.; Graca, I.; Carrer, H.; Barrett, D. H.; Teixeira-Neto, E.; Curvelo, A. A. S.; Rodella, C. B.; Rinaldi, R. Design of nickel supported on water-tolerant Nb_2O_5 catalysts for the hydrotreating of lignin streams obtained from lignin-first biorefining. *iScience* **2019**, *15*, 467−488.
(27) Li, L.; Dong, L.; Liu, X.; Guo, Y.; Wang, Y. Selective production of ethylbenzene from lignin oil over FeOx modified Ru/Nb_2O_5 catalyst. *Appl. Catal., B* **2020**, *260*, 118143.
(28) Emeis, C. A. Determination of integrated molar extinction coefficients for infrared absorption bands of pyridine adsorbed on solid acid catalysts. *J. Catal.* **1993**, *141*, 347−354.
(29) Guo, T.; Li, X.; Liu, X.; Guo, Y.; Wang, Y. Catalytic transformation of lignocellulosic biomass into arenes, 5-hydroxymethylfurfural, and furfural. *ChemSusChem* **2018**, *11*, 2758−2765.
(30) Wang, H.; Ruan, H.; Feng, M.; Qin, Y.; Job, H.; Luo, L.; Wang, C.; Engelhard, M. H.; Kuhn, E.; Chen, X.; Tucker, M. P.; Yang, B. One-pot process for hydrodeoxygenation of lignin to alkanes using Ru-based bimetallic and bifunctional catalysts supported on zeolite Y. *ChemSusChem* **2017**, *10*, 1846−1856.
(31) Yang, X.; Feng, M.; Choi, J.-S.; Meyer, H. M.; Yang, B. Depolymerization of corn stover lignin with bulk molybdenum carbide catalysts. *Fuel* **2019**, *244*, 528−535.
(32) Schofield, K. The enigmatic mechanism of the flame ionization detector: Its overlooked implications for fossil fuel combustion modeling. *Prog. Energy Combust. Sci.* **2008**, *34*, 330−350.
(33) Leal, G. F.; Barrett, D. H.; Carrer, H.; Figueroa, S. J. A.; Teixeira-Neto, E.; Curvelo, A. A. S.; Rodella, C. B. Morphological, structural, and chemical properties of thermally stable Ni-Nb_2O_5 for catalytic applications. *J. Phys. Chem. C* **2019**, *123*, 3130−3143.
(34) Nowak, I.; Ziolek, M. Niobium compounds: preparation, characterization, and application in heterogeneous catalysis. *Chem. Rev.* **1999**, *99*, 3603−3624.
(35) Jehng, J.-M.; Wachs, I. E. Structural chemistry and raman spectra of niobium oxides. *Chem. Mater.* **1991**, *3*, 100−107.
(36) Pittman, R. M.; Bell, A. T. Raman studies of the structure of Nb_2O_5/TiO_2. *J. Phys. Chem. A* **1993**, *97*, 12178−12185.
(37) Herval, L. K. S.; von Dreifus, D.; Rabelo, A. C.; Rodrigues, A. D.; Pereira, E. C.; Gobato, Y. G.; de Oliveira, A. J. A.; de Godoy, M. P. F. The role of defects on the structural and magnetic properties of Nb_2O_5. *J. Alloys Compd.* **2015**, *653*, 358−362.
(38) Sharma, P. K.; Saxena, N.; Roy, P. K.; Bhatt, A. Hydrogen generation by ethanol steam reforming over Rh/Al_2O_3 and Rh/$CeZrO_2$ catalysts: A comparative study. *Int. J. Hydrogen Energy* **2016**, *41*, 6123−6133.
(39) Wang, R.; Liu, X.; Chen, Y.; Li, W.; Xu, H. Effect of metal−support interaction on coking resistance of Rh-based catalysts in CH_4/CO_2 reforming. *Chin. J. Catal.* **2007**, *28*, 865−869.
(40) Jun, J.-W.; Suh, Y.-W.; Suh, D. J.; Lee, Y.-K. Strong metal-support interaction effect of Pt/Nb_2O_5 catalysts on aqueous phase hydrodeoxygenation of 1,6-hexanediol. *Catal. Today* **2018**, *302*, 108−114.
(41) Okuhara, T. Water-tolerant solid acid catalysts. *Chem. Rev.* **2002**, *102*, 3641−3666.
(42) Li, Y.; Jiang, J.; Zhu, C.; Li, L.; Li, Q.; Ding, Y.; Yang, W. The enhanced catalytic performance and stability of Rh/gamma-Al_2O_3 catalyst synthesized by atomic layer deposition (ALD) for methane dry reforming. *Materials* **2018**, *11*, 172−181.
(43) Wehner, P. S.; Mercer, P. N.; Apai, G. Interaction of H_2 and CO with $Rh_4(CO)_{12}$ supported on ZnO. *J. Catal.* **1983**, *84*, 244−247.
(44) Justin, P.; Hari Krishna Charan, P.; Ranga Rao, G. High performance Pt−Nb_2O_5/C electrocatalysts for methanol electrooxidation in acidic media. *Appl. Catal., B* **2010**, *100*, 510−515.
(45) Yu Yu Ko, H.; Mizuhata, M.; Kajinami, A.; Deki, S. Fabrication and characterization of Pt nanoparticles dispersed in Nb_2O_5 composite films by liquid phase deposition. *J. Mater. Chem.* **2002**, *12*, 1495−1499.
(46) Zhu, H.; Li, Y.; Zheng, X. In-situ DRIFTS study of CeO_2 supported Rh catalysts for N_2O decomposition. *Appl. Catal., A* **2019**, *571*, 89−95.
(47) Dal Santo, V.; Mondelli, C.; De Grandi, V.; Gallo, A.; Recchia, S.; Sordelli, L.; Psaro, R. Supported Rh catalysts for methane partial oxidation prepared by OM-CVD of Rh(acac)$(CO)_2$. *Appl. Catal., A* **2008**, *346*, 126−133.
(48) Matsubu, J. C.; Yang, V. N.; Christopher, P. Isolated metal active site concentration and stability control catalytic CO_2 reduction selectivity. *J. Am. Chem. Soc.* **2015**, *137*, 3076−3084.

https://dx.doi.org/10.1021/acssuschemeng.0c08478
ACS Sustainable Chem. Eng. 2021, 9, 3529−3541

(49) Kwon, Y.; Kim, T. Y.; Kwon, G.; Yi, J.; Lee, H. Selective activation of methane on single-atom catalyst of rhodium dispersed on zirconia for direct conversion. *J. Am. Chem. Soc.* **2017**, *139*, 17694−17699.
(50) Song, W.; Liu, Y.; Baráth, E.; Zhao, C.; Lercher, J. A. Synergistic effects of Ni and acid sites for hydrogenation and C−O bond cleavage of substituted phenols. *Green. Chem.* **2015**, *17*, 1204−1218.
(51) Guan, W.; Chen, X.; Hu, H.; Tsang, C.-W.; Zhang, J.; Lin, C. S. K.; Liang, C. Catalytic hydrogenolysis of lignin *β*-O-4 aryl ether compound and lignin to aromatics over Rh/Nb_2O_5 under low H_2 pressure. *Fuel Process. Technol.* **2020**, *203*, 106392−106401.
(52) Deepa, A. K.; Dhepe, P. L. Lignin depolymerization into aromatic monomers over solid acid catalysts. *ACS Catal.* **2015**, *5*, 365−379.
(53) Guo, H.; Zhang, B.; Qi, Z.; Li, C.; Ji, J.; Dai, T.; Wang, A.; Zhang, T. Valorization of lignin to simple phenolic compounds over tungsten carbide: Impact of lignin structure. *ChemSusChem* **2017**, *10*, 523−532.

https://dx.doi.org/10.1021/acssuschemeng.0c08478
ACS Sustainable Chem. Eng. 2021, 9, 3529−3541